

PLASMA DENSITY DETERMINED FROM THE SPACECRAFT POTENTIAL ON THE PARKER
SOLAR PROBE; TURBULENT DENSITY SPECTRA AND DENSITY FLUCTUATIONS IN
TRIGGERED ION ACOUSTIC WAVES

by F.S. Mozer¹, P.J. Kellogg²

1. Space Sciences Laboratory, University of California, Berkeley, USA

2. University of Minnesota, Minneapolis, Mn, USA

ABSTRACT

Power in density fluctuations at frequencies to 10,000 Hz have been determined through least squares fits of a function of the spacecraft potential to the plasma density measured on the Parker Solar Probe. The break in the $-5/3$ electric field and density spectra at kinetic scales is not well measured in the presence of higher frequency electrostatic waves that contain both electric field and density fluctuations of a few percent. An example of such fluctuations in triggered ion acoustic waves is presented.

INTRODUCTION

Since electric field antennas were first biased to make double probe electric field measurements in space plasmas [Mozer and Bruston, 1967] it has been recognized that the potential of the spacecraft body with respect to infinity, v_s , is related to the ambient plasma density [Knott et al, 1984]. This follows from the requirement that the net current to the spacecraft body is zero in equilibrium, or

$$I_{pe} - I_e + I_0 = 0 \tag{1}$$

where

I_{pe} is the photoemission current that escapes to infinity

I_e is the electron thermal current to the body and

I_0 represents all other currents, which are usually small.

When a spacecraft's photoemission exceeds its electron thermal current, the spacecraft charges positive with respect to infinity until the photocurrent that escapes to infinity, $i_{pe} \exp(-v_s/v_0)$, equals the plasma thermal current, where v_0 is the e-folding energy of the photoemission spectrum. Because the plasma thermal current is proportional to the plasma density, the requirement of no net current to the body produces a relationship between the potential of the spacecraft and the local plasma density. This relationship is complex because the photoemission does not always exceed the plasma electron current, the photoemission spectrum is not exactly an exponential [Scudder et al, 2000], secondary and thermal emission may be important on the Parker Solar Probe, etc.

In this work, it is assumed that these effects vary more slowly than the density such that calibrations of the potential-density relation on a short time scale allows density measurements from the spacecraft potential. A successful least squares procedure for determining the density is described in Appendix A, and the results of such density measurements are discussed below. The spacecraft potential data and waves discussed in this paper were produced by the FIELDS experiment on the Parker Solar Probe [Bale et al, 2016] while the proton plasma density was obtained from the SPAN instrument on the SWEAP detector package [Kasper et al, 2016].

DATA

Figure 1 compares the density spectra obtained from plasma measurements (the red curve) with that determined from the spacecraft potential (the blue curve) over a two-day period. The green line is a $-5/3$ spectrum [Kolmogorov, 1941]. The measured plasma density fell below the green line near and above 0.1 Hz because of the limited data rate of the plasma measurement. The green rectangle gives the frequency range covered by the least squares fitting routine. Outside the green rectangle, the two data sets are independent, such that the spacecraft potential produces the density spectrum to much higher frequencies than the direct measurement. This spectrum generally follows the $-5/3$ law except for the bump near 5 Hz, which is due to wave activity at this frequency. Without such knowledge, one might interpret the break at ~ 5 Hz as due to the beginning of the kinetic regime, which it is not.

This point is emphasized in Figure 2, which gives two spectra, the blue one during an interval without waves while the red one was taken when waves at several frequencies were present. While the break in the spectrum signifying the kinetic regime is ill defined by the red curve due to the waves, it is clearly seen to begin at about 5 Hz in the blue curve.

Figure 3 gives electric field (panel 3A) and density (panel 3B) spectra during two intervals, one with and one without waves above a few Hz. During the wave intervals (the black curves), there was electric field and density fluctuation power at 3-10 Hz and again at 100-1000 Hz. They are the triggered ion acoustic waves or TIAW [Mozer et al, 2021a, 2021b] that consist of several hundred Hz electrostatic waves that appear in bursts that are phase locked to the low frequency ion acoustic-like waves. During the time interval without such waves (the red curves), the main feature of the spectra was the existence of large electric field power below 10 Hz with no corresponding power in the density fluctuations. This is because these are electromagnetic waves that were

not present during the other interval. This result suggests the possibility that the electrostatic, triggered ion acoustic waves are anti-correlated with low frequency electromagnetic waves.

Figure 4 provides further information on the triggered ion acoustic waves during three time intervals of 10 minutes (panels 4A, 4B, and 4C), 1 second (panels 4D, 4E, and 4F), and 0.1 seconds (panels 4G, 4H, and 4I). During each time interval, the top plot (panels 4A, 4D, and 4G) gives the >100 Hz high pass filtered electric field, the middle plot (panels 4B, 4E, and 4H) gives the >0.5 Hz plasma density and the bottom plot (panels 4C, 4F, and 4I) gives the >100 Hz plasma density. The bursty electric field was as large as 50 mV/m and the density peaks of 60 cm^{-3} were about 2.5 percent of the background density. This suggests that the pressure associated with density fluctuations may be related to the core electron acceleration achieved by these waves [Mozer et al, 2021b]. A recent expansion instability theory [Kellogg, 2021] offers a possible explanation for the origin of these waves. It is also noted that these are the first density fluctuation spectra measured at frequencies as high as 10,000 Hz.

ACKNOWLEDGEMENTS

This work was supported by NASA contract NNN06AA01C. The authors acknowledge the extraordinary contributions of the Parker Solar Probe spacecraft engineering team at the Applied Physics Laboratory at Johns Hopkins University. The FIELDS experiment on the Parker Solar Probe was designed and developed under NASA contract NNN06AA01C. Our sincere thanks to S. Bale, P. Harvey, K. Goetz, and M. Pulupa for managing the spacecraft commanding, data processing, and data analysis, which has become a heavy load thanks to the complexity of the instruments and the orbit. We also acknowledge the SWEAP team for providing plasma density data.

ORCIDS

F. S. Mozer, <https://orcid.org/0000-0002-2011-8140>

P. J. Kellogg, <https://orcid.org/0000-0001-5223-689X>

REFERENCES

Bale, S.D., Goetz, K., Harvey, P. R., et al. 2016, *SSRv*, **204**, 49

Kasper, J. C. et al., 2016, *SSRv*, **204**, 131-186 (2016). DOI 10.1007/s11214-015-0206-3

Kellogg, P.J., 2021, *ApJ*, in publication

Knott, K., Decreau, P.M., Korth, A. et al, 1984, *Space Sci*, **32**, No. 2, 227-237

Kolmogorov, A.N. (1941) *Dokl. Akad. Nauk. SSSR* **30**, 299 Reprinted in *Proc. R. Soc. London A* **434**, 9 1991

Mozer, F.S. and Bruston, P., 1967, *J. Geophys. Res.*, **72** 1109-1114, <https://doi.org/10.1029/JZ072i003p01109>

Mozer, F.S., Vasko, I.Y., and Verniero, J.L., et al, 2021a, *ApJL*, **919**,L2 <https://doi.org/10.3847/2041-8213/ac2259>

Mozer, F.S., Cattell C.A., Halekas J., et al, 2021b, <http://arxiv.org/abs/2111.07161>

Scudder, J.D., Cao, X., and Mozer, F.S., 2000, *J.Geophys.Res.*, **105** no. A9, 21,281-21,294

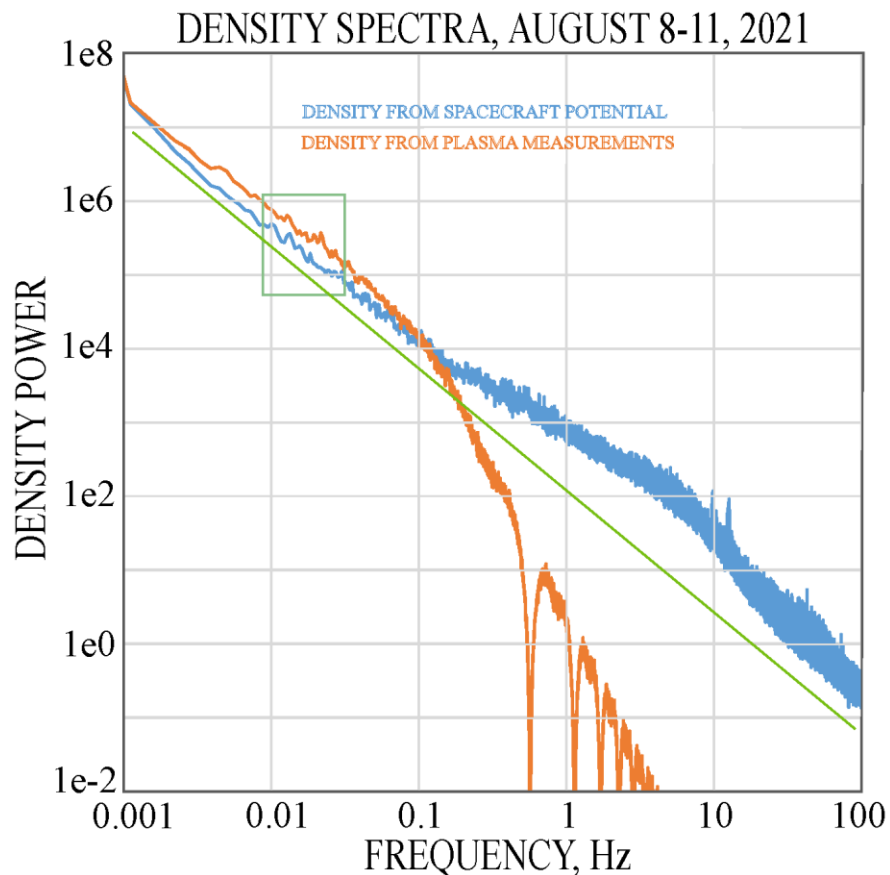


Figure 1. Plasma density measured by the plasma instruments on the Parker Solar Probe and derived from the measured spacecraft potential.

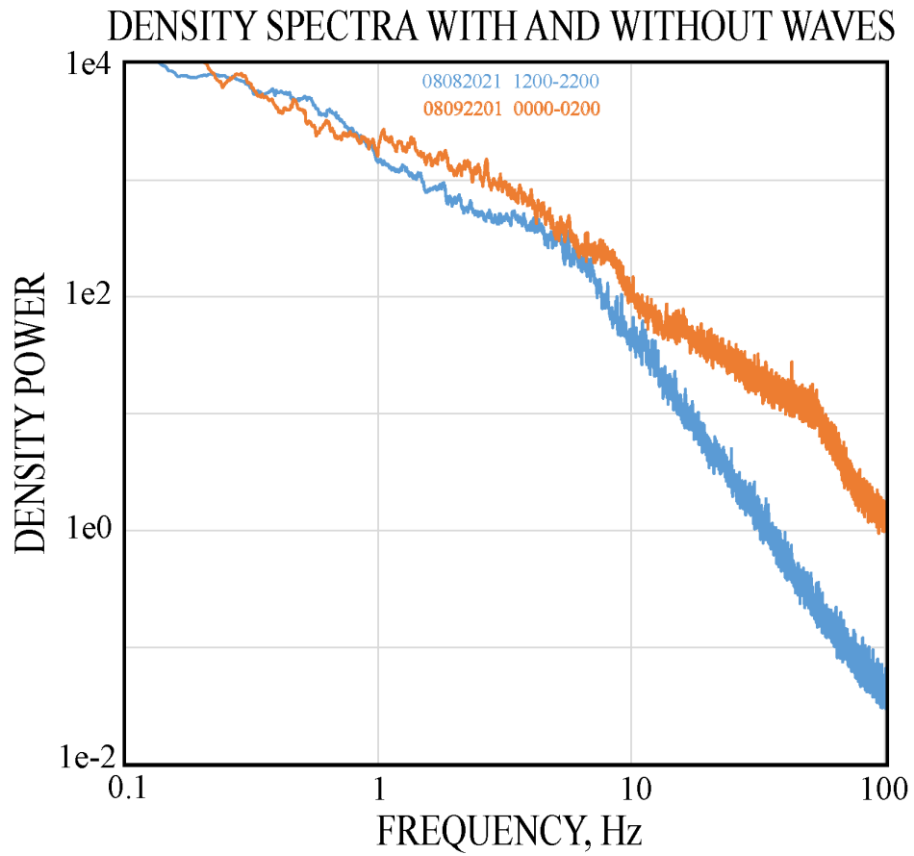


Figure 2. Density spectra during intervals with waves (the red curve) and without waves (the blue curve).

E-FIELD AND DENSITY SPECTRA WITH AND WITHOUT WAVES

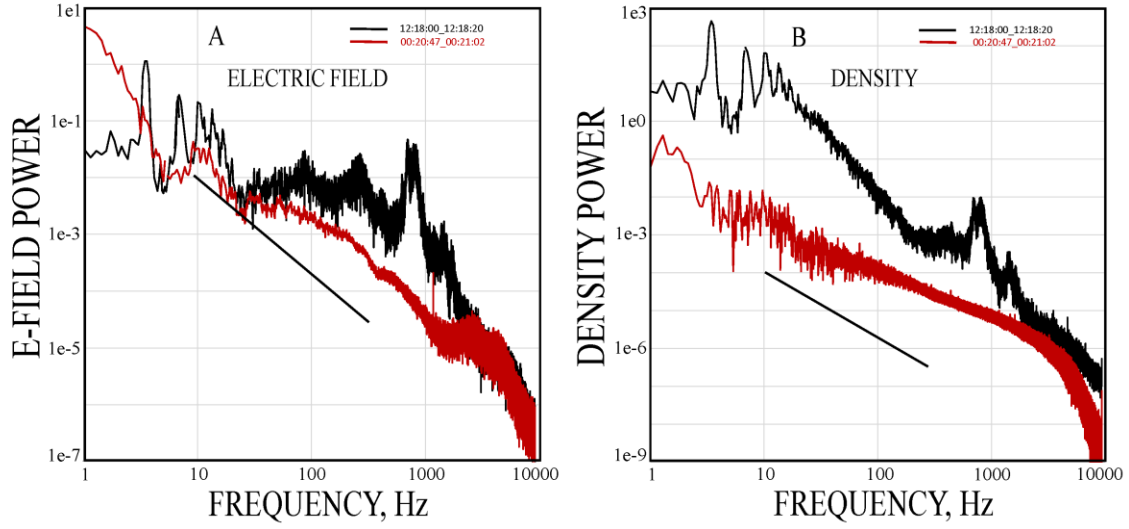


Figure 3. Electric field (panel 3A) and density (panel 3B) spectra during two intervals, one with waves (the black curves) and one without waves (the red curves). The straight lines have a $-5/3$ spectral slope.

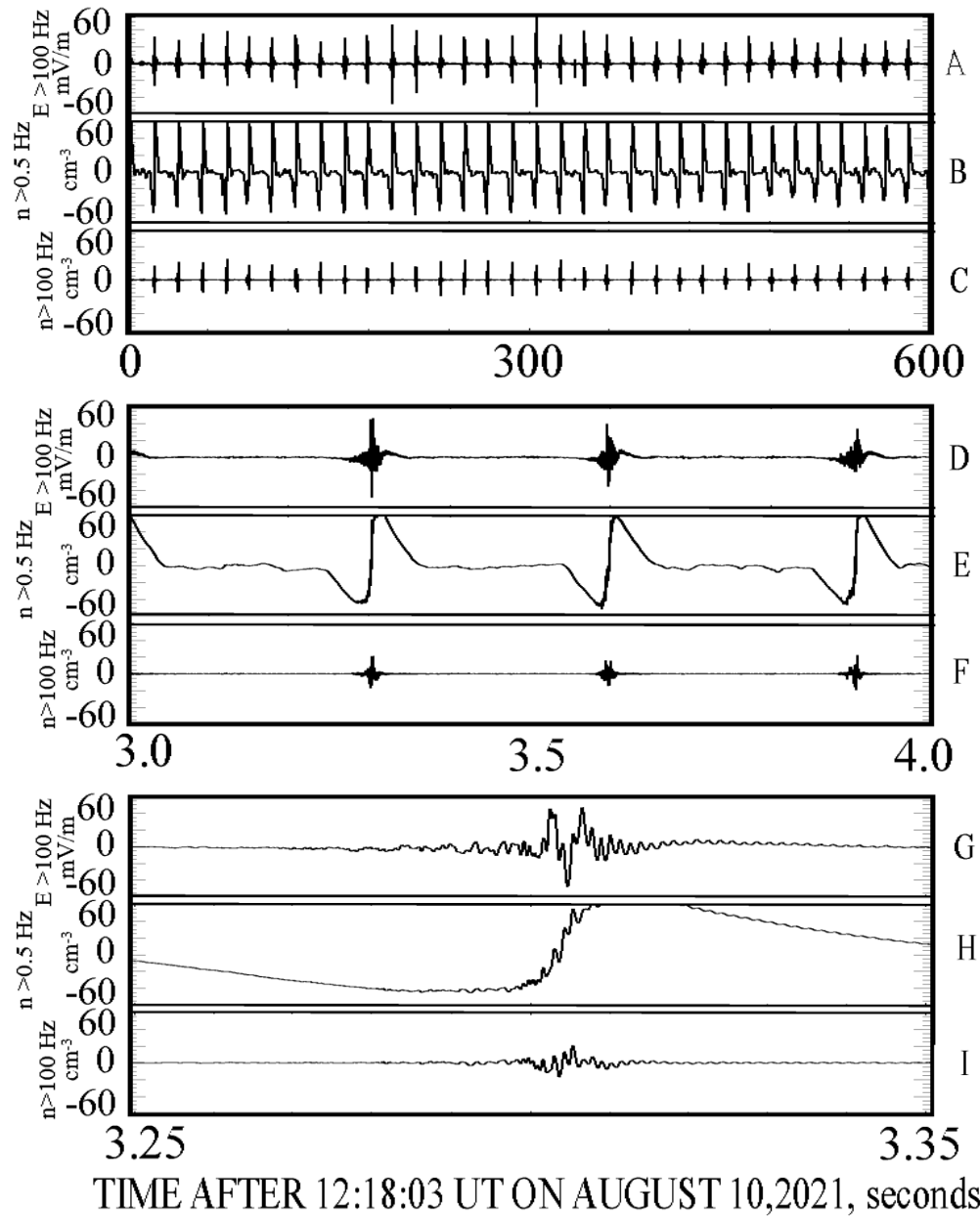


Figure 4. >100 Hz electric field (panels 4A, 4D, and 4G), >0.5 Hz plasma density fluctuations (panels 4B, 4E, and 4H) and >100 Hz plasma density fluctuations (panels 4C, 4F, and 4I) observed during time intervals of 10 minutes, 1 minute and 0.1 seconds, respectively.

APPENDIX A

The potential of a spacecraft surface with respect to infinity is determined from the requirement that the spacecraft charges until the net current to the body is zero. The current to the body is

$$I_{pe} - I_e + I_0 + I_1 = 0 \quad (1)$$

where

$$I_{pe} = \text{current due to escaping photoelectrons} \\ = i_0 A_s (R_0/R)^2 \exp(-v_s/v_0)$$

and

A_s = area of the sunlit spacecraft surface

R = distance from the Sun

v_s = potential of the spacecraft with respect to infinity, which is assumed to be positive because the photoelectron flux exceeds all other currents.

v_0 = e-folding energy of the assumed exponential photoelectron distribution.

$$I_e = \text{plasma electron thermal current} \\ = neA[kT/2\pi m]^{0.5} (1+ev/kT)$$

And

n = electron density

e = electron charge

A = spacecraft current collecting area

T = electron temperature

m = electron mass

$(1+ev/kT)$ = focusing factor

$I_0 = i_0 A_A$ = the bias current that is applied from the spacecraft to the antennas, where i_0 is a unit bias current and A_A is the area of the antennas.

I_1 = the current due to all other sources, including ions, secondary emission, thermal emission, etc.

Solving equation (1) after lumping all constants into K_1 , K_2 and K_3 gives

$$-v_s = K_1 \ln[nR^2(A/A_s)T^{0.5}] + K_2 \ln(1+ev/kT) + K_3 \ln[1+(i_0 A_A + I_1)/nAT^{0.5}(1+ev/kT)]$$

The measured spacecraft potential is $V_s = v_A - v_s$, where v_A is the potential of the antennas relative to infinity. Because the antennas are biased to be near zero potential, v_A is small but variable, so it is incorporated into the quantity B in equation (2) and $-v_s = V_s$. Because ev/kT is much less than 1, the K_2 term is small. Because A_A/A , the antenna area divided by the spacecraft area, is much less than 1, and because the neglected current, I_1 , may be small, the K_3 term is also small. The final result is thus,

$$V_s = A \cdot \ln[nR^2(A/A_s)T^{0.5}] + B \quad (2)$$

where the constant, B, includes the terms associated with v_A , K_2 and K_3 .

On spinning spacecraft the spacecraft total area divided by the sunlit area, A/A_s , varies with the spin period, so the above equation does not reproduce the electron density from the spacecraft potential at frequencies greater than the spin frequency unless this factor is accounted for. However, the Parker Solar Probe keeps the same surface pointed towards the Sun throughout each perigee pass, so the logarithm of the area ratio is constant and can be included as part of the constant, B. This gives

$$V_s = A \cdot \ln[nR^2T^{0.5}] + B \quad (3)$$

Equation (3) may be validated by comparing V_s with $\ln[nR^2T^{0.5}]$, as is done in Figure A1 where it is seen that the two quantities appear to be related.

In principle, A and B should be nearly constant. However, they are not constants because the neglected terms are not truly constant or small. For example, the secondary emission from the spacecraft body may be significant and variable, the photoelectron spectrum may deviate from an exponential, the area of the spacecraft body is not infinitely large compared to the area of the antennas, the photoemission of the heat shield may vary with temperature, the potential of the antennas with respect to infinity may not be small, etc. In addition, the Span measurements that produce the density, n , are noisy and they sometimes underestimate the actual density. These shortcomings are overcome partially by incorporating these error terms into the constants A and B and doing least squares fits to find A and B on time scales during which the error terms are roughly constant. Thus, A and B are determined from four minute least squares fits of equation (2), using 30 second averaged measurements of spacecraft potential, electron temperature, density, and the spacecraft location. Following this step, the two constants are coupled with the highest time resolution measurements of the spacecraft

potential to produce high time resolution plasma density from the spacecraft potential. The 30 second averaging time scale results from the desire to average many samples of the noisy <1 Hz plasma data into a single analysis data point. The four minute least squares fitting time scale results from the desire to have eight data points in each least squares fit.

Figure A2 displays the results of such a least squares fit. In panel A2A, the plasma density measured by the plasma instrument is shown as the red curve and the density determined from the higher time and frequency resolution spacecraft potential measurements is the black curve. The two curves are approximately identical except for the higher frequency variations determined from the spacecraft potential. The bottom panel of Figure A2 displays these higher frequency variations after the data is high-pass filtered at 0.5 Hz. The density fluctuations, appearing as blobs in time in panel A2B, have amplitudes as large as 500 nT when the background density is less than 4000 nT, so large density fluctuations are present.

The above derivation applies when the photocurrent exceeds the plasma current, for which case the least squares coefficient A is positive. While this ratio is usually greater than one, there are times when the opposite is true. At such times, all of the photocurrent from the spacecraft escapes to infinity and its magnitude does not depend on the potential of the spacecraft. However, at such times, the electron thermal current decreases with increasingly negative potential of the spacecraft with respect to infinity. If the thermal current spectrum decreases exponentially with this potential, the above derivation applies, in which case the e-folding potential becomes that of the thermal electron distribution in place of the photoemission spectrum. In this case, the least squares coefficient A would be negative and coefficient B would change because of the different e-folding energy. These effects are seen in Figure A3, which plots the coefficients A and B for the two days of interest.

A conceivable error in the determination of the plasma density from the spacecraft potential is that neither the photoelectron nor the thermal plasma spectra are exponentials over a wide energy range. However, they may be approximated as exponentials over the confined energy and time interval of each least squares fit. In this way, variations of the two spectra are accommodated as variations of the least squares coefficients.

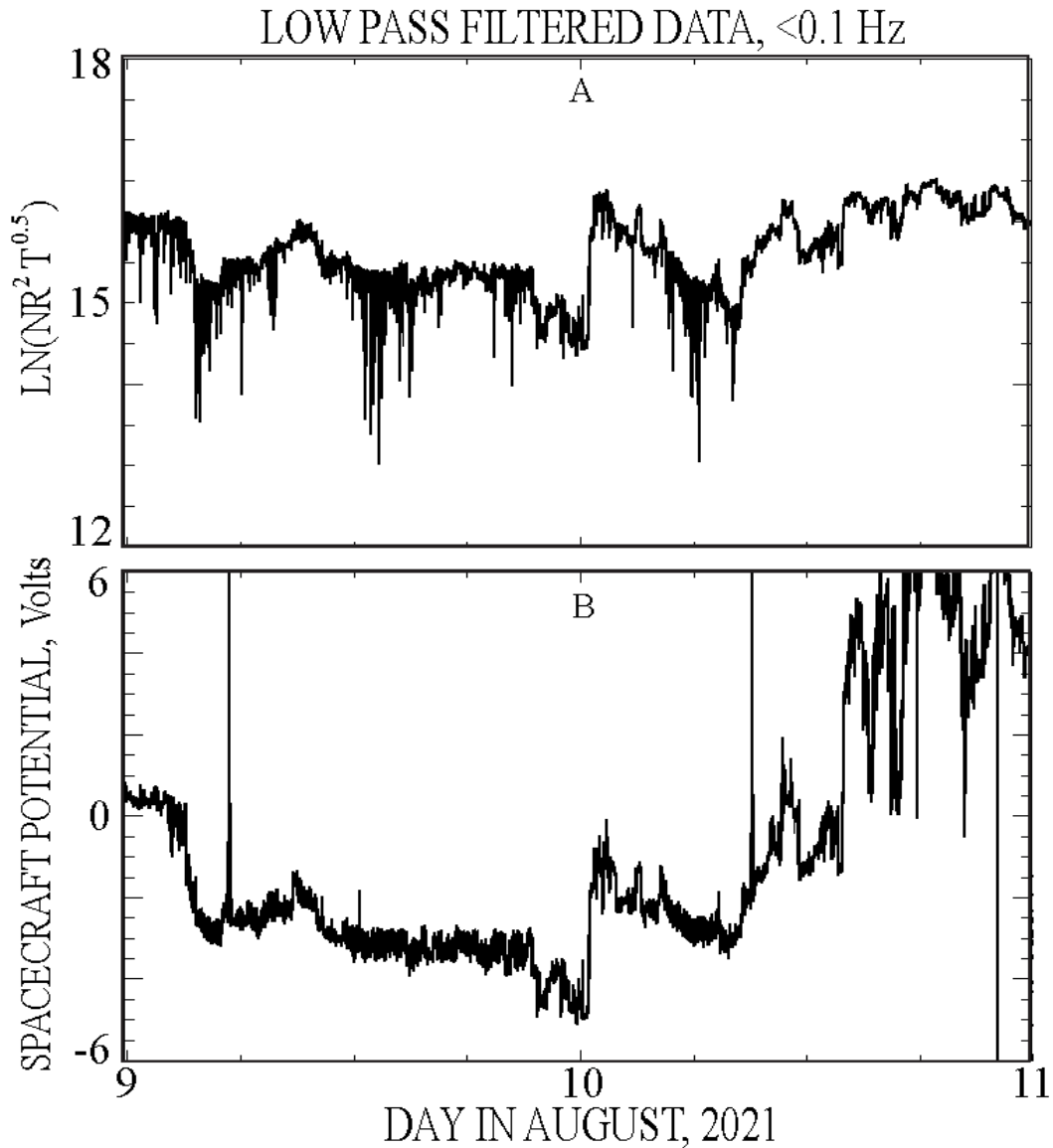


Figure A1. Comparison of $\ln[nR^2T^{0.5}]$ in panel A with the spacecraft potential in panel B. The dropouts in panel A are due to density measurement problems and the large vertical lines in panel B are due to dust hits. The general correlation between the two quantities and the detailed differences in the amplitudes of their changes show that equation (2) can provide a good fit of the two data sets.

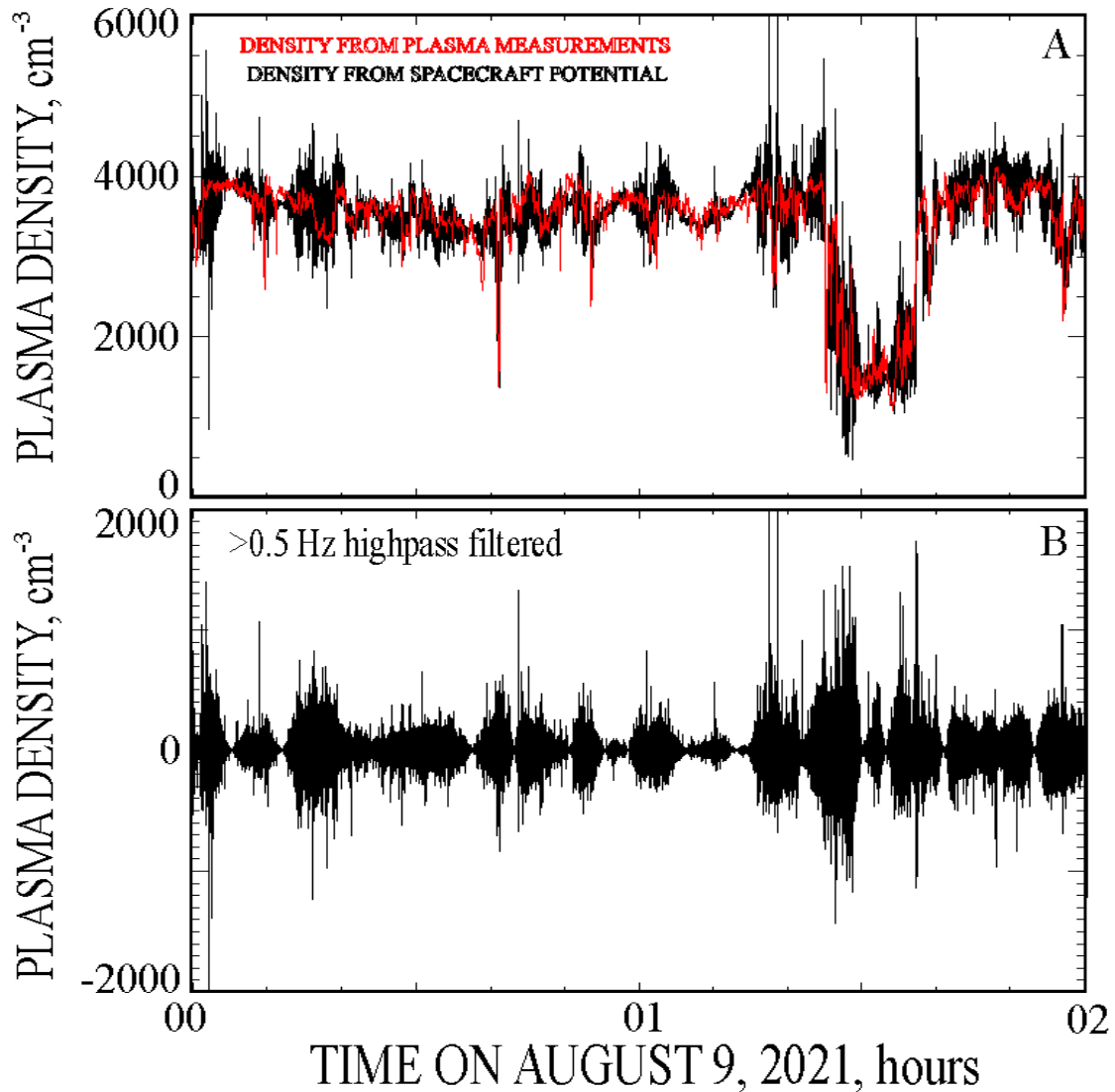


Figure A2. Panel A provides a two-day comparison between the plasma density measured by the plasma instruments (red) and the density obtained from the spacecraft potential (black). The black curve has a higher frequency response. Its high pass filtered data, in panel B, shows that the density fluctuations occurred in bursts and that the density fluctuations were sometimes greater than 10% of the density.

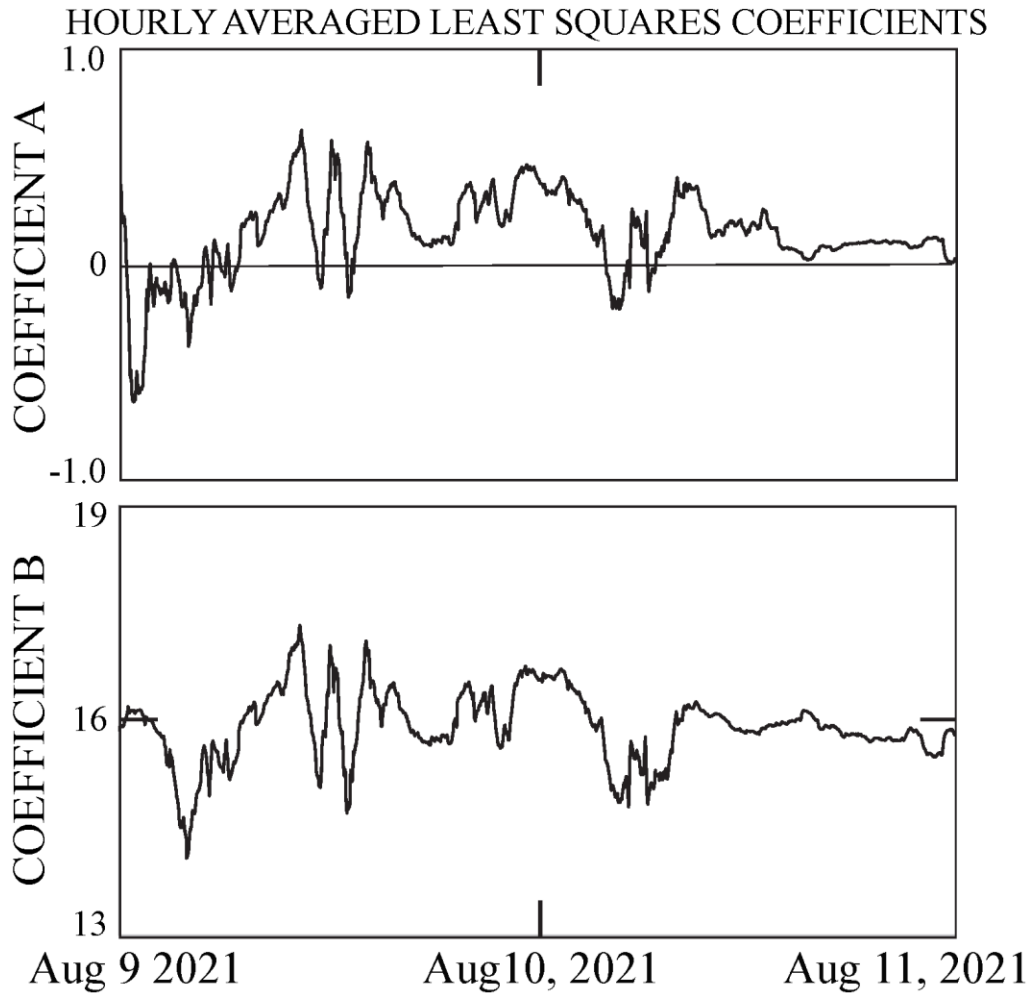


Figure A3. Coefficients obtained from least squares fitting equation 2. Note that coefficient A is positive when the photoemission exceeds the plasma thermal current (the normal case) and negative in the opposite situation.